JOWRM

Journal of Water Resources Management

Journal homepage: https://journal.water.gov.my

e-ISSN: 2811-3578

Numerical Analysis Study of Debris Flow Impact by Smoothed Particle Hydrodynamics

Muhammad Khairi A.Wahab [1,a], Mohd Remy Rozainy Mohd Arif Zainol [2,b*], Mohamad Aizat Abas [3,c], Norizham Abdul Razak [4,d]

[1] School of Civil Engineering,
Engineering Campus, Universiti Sains Malaysia, Nibong Tebal, 14300, MALAYSIA

[2] River Engineering and Urban Drainage Research Centre (REDAC),
Engineering Campus, Universiti Sains Malaysia, Seri Ampangan, Nibong Tebal, 14300, MALAYSIA

[3] School of Mechanical Engineering,
Engineering Campus, Universiti Sains Malaysia, Nibong Tebal, 14300, MALAYSIA

[4] School of Aerospace Engineering,
Engineering Campus, Universiti Sains Malaysia, Nibong Tebal, 14300, MALAYSIA

*Corresponding Author

Email: [a]muhdkhairi88@gmail.com, [b]ceremy@usm.my, [c]aizatabas@usm.my, [d]norizham@usm.my

Received 07 March 2025;
Accepted 07 June 2025;
Available online 28 June 2025

Abstract: Debris flows are highly destructive natural events that occur in mountainous regions, causing widespread damage to both the environment and communities. These events can lead to severe casualties and environmental degradation, making it crucial to thoroughly assess their impacts to improve mitigation strategies and increase understanding of their consequences. This paper presents an evaluation of debris flow impact on a deposition board through numerical simulation. The study investigates two scenarios based on flume slope steepness of 25° with fully and half-open gates. Limestone particles, with a total volume of 1×10^3 m³, were used to simulate debris, released with water from a tank onto a 1 m² deposition board. The force exerted by the particle flow on a building block located on the board was measured. The simulations revealed that the maximum forces exerted were 55.2 N for the fully open gate and 47.3 N for the half-open gate. These findings highlight the potential risks posed by debris flows in real-world situations. The results are valuable for risk assessments, the development of safety guidelines, and reducing the risk of debris flows in vulnerable areas.

Keywords: Debris flow, SPH, Risk assessment, Impact force, Computational

1. Introduction

Debris flow is a natural occurrence occurring in hilly areas with elevated valleys or streams that experience substantial annual precipitation. This occurrence is among the most perilous natural events affecting mountainous regions due to its substantial debris volume and prolonged runout. [1]. Debris flow is a mixture of solids, soil, wood, gravel, pebbles, snow, ice, and water that moves down slopes due to gravity [2]. These occurrences often lead to significant destruction of property, loss of life, and changes in the physical features of riverbeds and mountain slopes [1], [3], [4].

Significant rainfall led to serious flooding and landslides in many regions of the country [5], [6]. Debris flows can result from various mechanisms, including heavy rainfall that transforms landslides into rapidly moving liquid sediments [6]–[8]. Debris flow development involves three stages: initiation area, propagation zone, and deposition area [1], [9].

The initiation phase involves the release of the initial large amounts. The most common type is debris flow, which is triggered by either a single huge landslide or a sequence of smaller landslides. They occur when a landslide or debris slide transitions into a debris flow. Mobilization is the transformation of a stationary mass of liquid soil, silt, or rock into debris flows. Surface-water runoff significantly contributes to the formation of a debris flow [9]–[13]. Debris flows can result from steep channels containing a large amount of sediment, shallow landslides, and common occurrences in high-altitude areas [14]–[16]. The triggered process is influenced by various parameters like as geomorphology, geotechnical properties of slope angle, hydrological elements, and geological conditions[8], [17]. Studying and comprehending the causes of debris flow start

**Corresponding author: ceremy@usm.my*

under different conditions is crucial for creating strategies to mitigate debris flow [18], [19].

Smoothed Particle Hydrodynamics has emerged as a powerful computational technique for simulating complex fluid dynamics, including the behavior of debris flows. Recent studies have explored the application of SPH to debris flow modeling, providing valuable insights into the dynamics of these hazardous events [20], [21].

One case study focused on a debris flow event in the Loess Plateau region of China, where researchers utilized the FLO-2D model, a non-Newtonian fluid-based approach, to simulate the discharges of debris flow in the Huaxi Gully under both operational and dam-failure conditions [21]. The study demonstrated the effectiveness of the FLO-2D model in predicting the behavior of debris flows, highlighting the potential of SPH-based methods for hazard assessment and mitigation.

Another recent study investigated the use of SPH to model the hydrodynamic forces and water surface elevation associated with debris impacts. The researchers found that while the SPH model was able to reasonably replicate the hydrodynamic forces and water surface elevation, it struggled to accurately capture the large debris impact forces observed in experimental testing [22]–[24] . However, the study also suggested that coastal forests could potentially provide protection against floating debris, which is an important consideration for debris flow risk management [25].

More recently, a study focused on the Vajont landslide in the Dolomites region, where researchers applied the open-source SPH model DualSPHysics to simulate the debris flow that resulted from the catastrophic event [26]. The study provided valuable insights into the propagation speed and traveled distances of the debris flow, which are crucial for assessing the risk and proposing mitigation strategies. These studies demonstrate the growing applicability of SPH-based modeling in the field of debris flow research. By incorporating recent advances in SPH techniques and leveraging the capabilities of non-Newtonian fluid models, researchers are able to gain a more comprehensive understanding of the complex dynamics of debris flows, ultimately contributing to improved hazard assessment and risk management strategies [23], [26]–[28].

The application of SPH to debris flow modeling is an active area of research, with studies exploring a range of scenarios and conditions. By incorporating recent findings from these studies, researchers can further develop and refine SPH-based approaches to better understand and predict the complex behavior of debris flows.

1.1 SPH Formulation

The SPH integral interpolation function f(x) can precisely simulate continuous fluid motion using several particles with mass and momentum [29]–[31]. The function f(x) at point (x, y, z) is estimated using the expression provided:

$$f(\boldsymbol{x}) = \int_{\Omega} f(\boldsymbol{x}')W(\boldsymbol{x}-\boldsymbol{x}', h)d\boldsymbol{x}' \qquad (1)$$

Ω denotes the computational domain at position x, is the volume element over the domain, is the weight equation or smooth kernel function, and h is the smooth length that specifies the size of the computational domain of the kernel function.

Numerical approximations of the integrals are computed by summing the contributions from neighboring particles inside the specified region, with the subscript indicating an individual particle.

$$f(\boldsymbol{x_a}) \approx \sum_b f(\boldsymbol{x}_a)W(\boldsymbol{x}_a-\boldsymbol{x}_b, h)\Delta v_b \qquad (2)$$

Where Δv_b represents the volume of neighboring particle (b), $\Delta v_b = \frac{m_b}{\rho_b}$, m is the mass and ρ is density.

Where the subscript represents a single particle, it then becomes: -

$$f(\boldsymbol{x_a}) \approx \sum_b f(\boldsymbol{x}_a)\frac{m_b}{\rho_b}W(\boldsymbol{x}_a-\boldsymbol{x}_b, h) \qquad (3)$$

The selection of smoothing kernel will greatly affect the performance of an SPH model. Kernel functions play a crucial role in the Smoothed Particle Hydrodynamics (SPH) approach, impacting its computational correctness and stability. Consequently, they have been extensively researched by numerous scholars [32]. According to Yang (2014) [33], the stability of Smoothed Particle Hydrodynamics (SPH) depends on the second derivative of the kernel function. Kernels are expressed as a function of the dimensionless distance between particles (q). DualSPHysics offers two kernels: Cubic Spline and Quintic. Users can choose from these kernel definitions with flexibility.

2. METHODOLOGY

2.1 Validation of the Developed SPH Model

Rheological parameters for fluid phase are the default parameter and for the sediment phase obtained from the factory in Ipoh, Malaysia. The interaction of different debris materials with flow dynamics and deposition patterns is a complex phenomenon influenced by various factors, including particle size, composition, and the physical properties of the debris. Understanding these interactions is crucial for predicting the behavior of debris flows, which can have significant implications for erosion, sediment transport, and hazard assessment. One of the primary factors affecting flow dynamics is the grain size distribution of debris materials. Johnson (2012) demonstrated that in geophysical mass flows, the segregation of grain sizes leads to the formation of distinct layers, with coarser particles settling at the base of the flow [34]. This segregation can significantly alter the flow's rheological properties, affecting its velocity and the patterns of deposition. Coarser materials tend to create a more stable base, while finer particles can enhance fluidity, leading to different flow behaviors and deposition characteristics.

Before conducting the studies, a comprehensive characterisation of the limestone was performed to ascertain its particle size. To achieve the requisite particle size for the medium, approximately 1 kilogram of limestone was subjected to sieving with a sieve shaker. The particles were filtered to pass through a 1.18 mm aperture while being retained within a 2 mm size range. The limestone utilised in the experiment have a density of 2573 kg/m³.

In simulation, the grid simulation study investigated the effects of different grid sizes (coarse, medium, and fine) on accuracy and computational efficiency for three slope angles (15°, 20°, 25°) and three water levels. The inter-particle distances for the grids were 0.01m (coarse), 0.009m

(medium), and 0.008m (fine). Importantly, only one particle size was tested throughout the entire study and all cases to ensure consistency and control over variables, as introducing different particle sizes could complicate the analysis and obscure the effects of grid resolution on simulation outcomes. By focusing on grid size alone, the study could more clearly assess its influence on accuracy and computational requirements. As the grid size became finer, the total number of elements and simulation runtime increased, but accuracy improved. For example, with a 15° slope and 0.105 water level (WL), the velocity differences from experimental data were 15.49% for the coarse grid, 11.86% for the medium grid, and 8.81% for the fine grid. This pattern continued for other slopes and water levels, where finer grids yielded smaller percentage differences in velocity compared to experimental results. Despite the increased computational time, the fine grid (dx = 0.008) was ultimately chosen for its superior accuracy and balance between computational efficiency and precision. The study demonstrated that finer grids provide more accurate results, although they require greater computational resources. Testing a single particle size throughout the study allowed the research to isolate the impact of grid resolution, leading to clearer conclusions on the grid's role in simulation accuracy.

One parameter value for sediment phase (viscosity) and were gathered from other researchers and through trial and error within a reasonable parameter range to ensure that the debris flow deposition for numerical is more closely aligned to the experimental conditions. This is a popular method for obtaining unknown simulation parameters [35]–[40].

The Kernel function is chosen for this study due to its advantageous properties that enhance simulation accuracy and stability. This kernel function, characterized by its higher-order interpolation capabilities, provides several benefits that make it a compelling choice for various fluid dynamics applications. One of the primary advantages of the quintic kernel is its ability to achieve a high degree of accuracy in approximating fluid properties. As noted by Xiang and Chen, the quintic kernel function improves inter-particle force stabilization and consistency in simulations, particularly in compressive states, by ensuring a non-negative second-order derivative Xiang & Chen (2016) [41]. This characteristic is crucial for maintaining stability in SPH simulations, especially when dealing with complex fluid interactions.

Moreover, the quintic kernel has been shown to effectively reduce temperature differences in regions close to boundaries, as demonstrated by Filho (2016) [42]. This reduction in temperature discrepancies is vital for accurately modeling thermal processes in fluid dynamics, where boundary conditions can significantly influence the overall behavior of the system. The quintic kernel's performance in this regard highlights its utility in applications requiring precise thermal management.

The accuracy of the SPH simulations was validated through a comparison between the obtained velocity data and PIV, while the shape of the deposition from SPH was validated by comparing it with the shape observed in the experiment. The level of accuracy was assessed by considering the percentage difference for each case among the 12 cases. Validation in numerical analysis is essential for verifying the accuracy and dependability of computational models by comparing their predictions with experimental measurements. Researchers can enhance the reliability of computational models and make well-informed decisions by integrating numerical simulations with experimental data. Specific criteria or standards are frequently used to verify the reliability and validity of findings. The criteria are used to evaluate the quality and reliability of the results. The criteria are categorized into four groups: A (<10%), B (10%-20%), C (20%-30%), and D (>50%). Table 1 displays the accuracy levels for each category: A for good accuracy, B for acceptable accuracy, C for marginal accuracy, and D for low accuracy [43].

Table 1 - Accuracy based on relative error

Category	Range (%)	Quality
A	<10	Good
B	10-30	Acceptable
C	30-40	Marginal
D	50>	Poor

2.2 Experimental Setup for Debris Flow Model Test for Validation

Measuring the relevant parameters of debris flow in the field is challenging due to the catastrophic nature of these occurrences. The laboratory model test is often used to study debris flow deposition. The study's framework consisted of three main components: a water tank, a flume, and a deposition board. The case determines the degree that the flume's slope should be. Before the test procedure is carried out, the flume's slope is determined. The three slope levels used in this study were 15°, 20°, and 25°. This was selected because debris flows only happen in the 15° to 25° range [10], [44], [45]. The water tank was filled manually using a pump mechanism, with the flow being controlled by a butterfly valve attached to the pipe. The model's physical dimensions were as follows: The model had dimensions of 4.55 m x 1.1 m x 1.5 m. The water tank measured 1 m x 1 m x 1 m. The flume was 2.5 m x 0.1 m x 0.01 m. The deposition board was 1 m x 1 m. The model was constructed using a 10 mm thick polyvinyl chloride (PVC) sheet. Refer to Fig. 1 for a visual representation of the model's geometry.

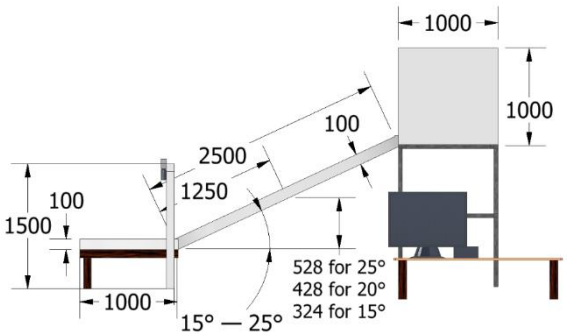

Fig. 1 - The geometry of the physical model with PIV set-up

The validation involved twelve cases that were exposed to different water levels, flume angles, and water gate openings. The layout of these case studies and their respective operations is detailed in Table 2, offering a thorough summary of the methods used in this section.

Table 2 - Experiments that have been undertaken

Case Study	Flume Degree (°)	Water Level (mm)	Gate Opening
1	15	120	Half
2	15	120	Full

3	15	150	Half
4	15	150	Full
5	20	120	Half
6	20	120	Full
7	20	150	Half
8	20	150	Full
9	25	120	Half
10	25	120	Full
11	25	150	Half
12	25	150	Full

The results of experiments and numerical analysis by comparing the deposition patterns. This process is intended to determine the similarity of their shapes. A sediment viscosity of 1.0 was incorporated into the simulation via several trial-and-error procedures within a tolerable parameter range. Approximately three numerical scenarios closely mimic the experiment's deposition pattern out of a total of 12. Table 3 features highlighted cases, specifically Case 2, Case 8, and Case 9, which are underlined in green and displayed in this section. To calculate the percentage of sediment deposition in the region, subtract the plane area from the entire area of the deposition board (measured 1000 x 1000 mm or 1 x 106 mm^2), and then multiply the result by 100. This enables the calculation of the proportion of sediment accumulated on the sedimentation board.

Table 3 - Relative error in the planar area of the numerical data compared to the experimental data

Case No.	Planar Area (mm^2)		Relative error (%)
	Experimental (x 10^3)	SPH (x 10^3)	
1	536.79	594.78	10.25
2	436.93	450.14	2.98
3	488.42	547.41	11.39
4	402.34	451.66	11.55
5	461.38	519.03	11.76
6	447.06	493.72	9.92
7	415.86	462.13	10.54
8	290.03	320.00	9.83
9	367.62	408.24	7.51
10	321.46	364.98	12.68
11	485.07	550.74	14.05
12	298.70	331.70	10.47

2.3 SPH Simulation on Debris Flow Impact

SPH has shown that it can predict occurrences and provide a good degree of agreement between observational data. Due to this, SPH is able to compute pressure, the hydrodynamic force acting on a static object, and the velocity of the two phases of debris flow. DualSPhysics was used to simulate two cases with different geometries compared to previous cases, namely Case 1A and 1B.

For case 1A, the size of the width and height of the flume are doubled to 0.2m width and 0.2m height. The sediment size is increased to 0.2 width, 0.5 long and 0.1m height. The water level in the tank is raised to 200mm. A new geometry block is added to the deposition board and called as a building to see the force from the debris flow effect. The new geometry of model is shown in Fig. 2.

For Case 1B, the flume and sediment sizes are the same as Case 1A. The only change to the model is the operation of the water gate, which is half open.

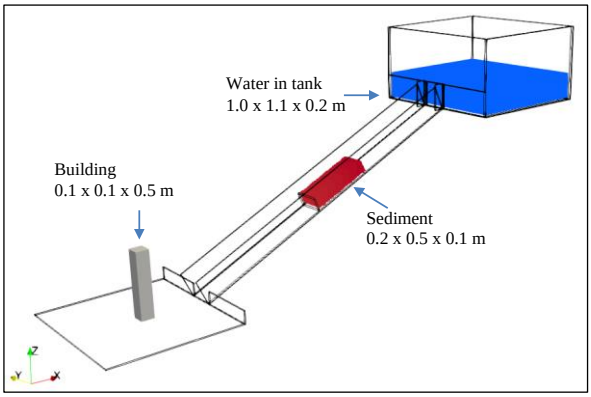

Fig. 2 - Geometry for debris flow impact model

One monitoring point, Point A at (0.55, 0.65, 0.05) in YXZ coordinate measured the velocity in front of the building block. The locations of these monitoring points are shown in Fig. 3.

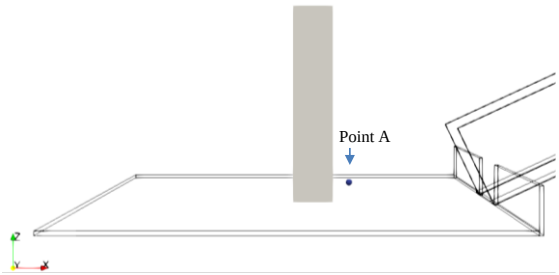

Fig. 3 - The measuring point in the model for Case 1A and 1B

3. RESULT AND DISCUSSION

3.1 Case 1A

This case was operated at water level 200 m and the gate is fully open for 5s at a slope angle of 25 º. The entire forces on the building block by fluid and sediment has been plotted on Fig. 4. It can be seen on the figure that debris contacts the building block at 1.47 s. The maximum force value recorded is 55.2N at 1.96 s and mean is 5.45 N.

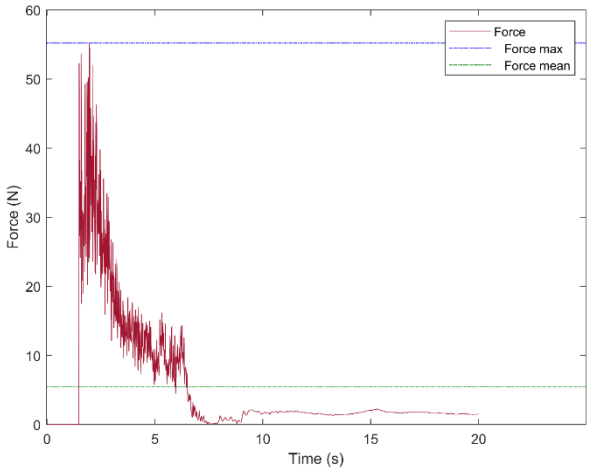

Fig. 4 - Plot of the forces on Building from Case 1A

In Fig. 5, the velocity for point A is plotted against time(s). From the figure, it can be seen that the debris flow reached at 1.46 s, the maximum velocity recorded is 3.44 cm/s at 3.46 s and the mean velocity is 0.41 cm/s. The velocity decreased rapidly at 6.24 s then gradually decreased until 20 s because the gate was closed and the water flow decreased until the 20 s.

This velocity magnitude graph showing three major stages; the acceleration stage after the mixture passes from the flume and reaches the monitoring point, the deceleration stage due to the viscosity of the mixture, and the propagation stage with a steady velocity. The pattern for velocity is approximately identical as force indicating that graph when velocity is high, force is high.

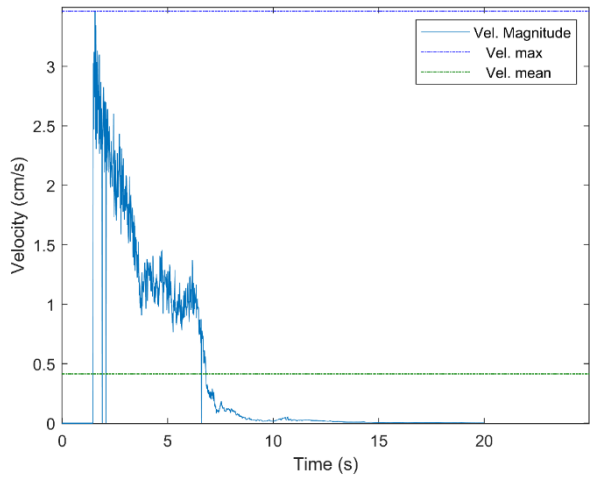

Fig. 5 - Velocity against time plotted on point A for Case 1

Fig. 6 is a snapshot of the debris flow for Case 1A through the simulation. As shown in the figure, the water gate open at t=0.10 s, the fluid contacts the sediment at 0.56 s, then the two-phase mixture moves downstream to the deposition board. At t=1.34 s, the mixture reaches the deposition and contacts the building block at t=1.46 s. The mixture forms a flow shape at t=1.56 s after the collision with the building block. The mixture has started to fill the deposition board at t=4.00. At t=5.10 s, the water gate closes, it can be seen that the mixture flow velocity has started to decrease and the end result of the debris flow at t=20.00 s.

Fig. 7 showing the debris pattern simulated by DualSPHysics on the deposition board. The sediment is represented by the black particles while the blue particles represent the water. A velocity reading of 0.0e-00 cm/s indicates that the particles have stopped moving and have settled down. The results of the study showed that the shape that exhibited a uniform runout pattern without channels on the fan and the building block in the middle-facilitated deposition more effectively and evenly to the left and right. Consequently, the presence of an obstruction object, such as the building block, appears to play a significant role in the deposition pattern.

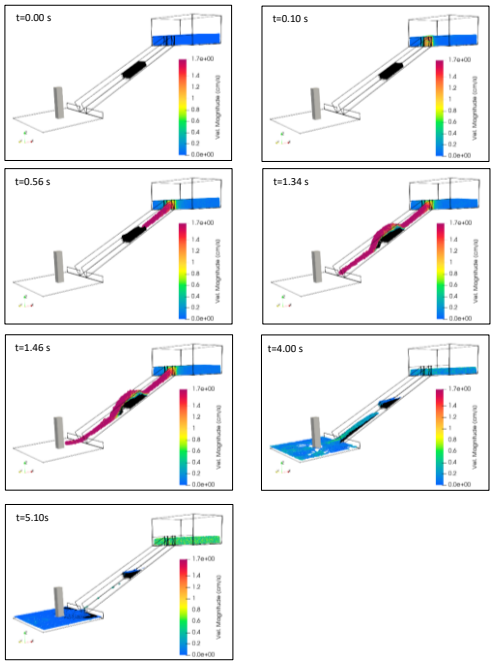

Fig. 6 - Velocity field of the simulation in different flow instants for Case 1A

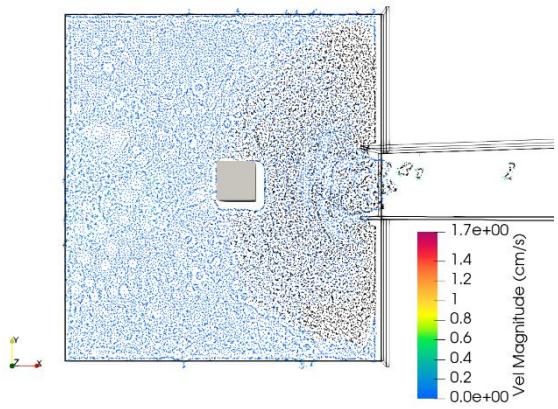

Fig. 7 - Simulation result of the debris deposition at t=20.00 s for Case 1A

In Fig. 8, the velocity for point A is plotted against time(s). From the figure, it can be seen that the debris flow reached at 1.52 s, the maximum velocity recorded is 3.33 cm/s at 3.51 s and the mean velocity is 0.31 cm/s. The velocity

decreased rapidly at 6.45 s then gradually decreased until 20 s because the gate was closed and the water flow decreased until the 20 s.

The velocity magnitude graph illustrates three main stages: acceleration once the mixture moves from the flume to the monitoring point, slowing caused by the mixture's viscosity, and propagation at a constant velocity. The velocity pattern closely mirrors the force pattern, suggesting that when velocity is high, force is also high.

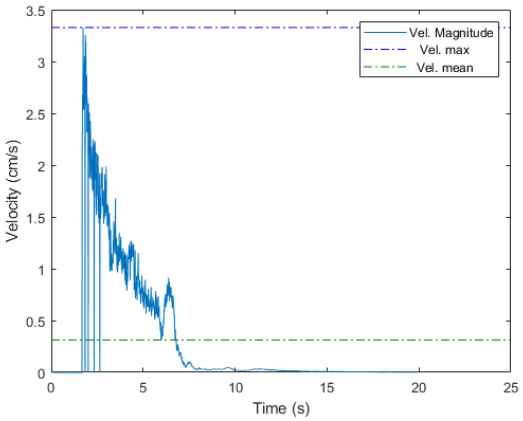

Fig. 8 - Velocity against time plotted on point A for Case 1B

Fig. 9 is a snapshot of the debris flow for Case 1B through the simulation. As shown in the figure, the water gate open at t=0.10 s, the fluid contacts the sediment at 0.60 s, then the two-phase mixture moves downstream to the deposition board. At t=1.34 s, the mixture reaches the deposition and contacts the building block at t=1.66 s. The mixture forms a flow shape at t=1.80 s after the collision with the building block. The mixture has started to fill the deposition board at t=4.00. At t=5.10 s, the water gate closes, it can be seen that the mixture flow velocity has started to decrease and the end result of the debris flow at t=20.00 s.

Fig. 10 showing the debris pattern simulated by DualSPHysics on the deposition board. The sediment is represented by the black particles while the blue particles represent the water. A velocity reading of 0.0e-00 cm/s indicates that the particles have stopped moving and have settled down. The results of the study showed that the shape that exhibited a uniform runout pattern without channels on the fan and the building block in the middle-facilitated deposition more effectively and evenly to the left and right. Consequently, the presence of an obstruction object, such as the building block, appears to play a significant role in the deposition pattern.

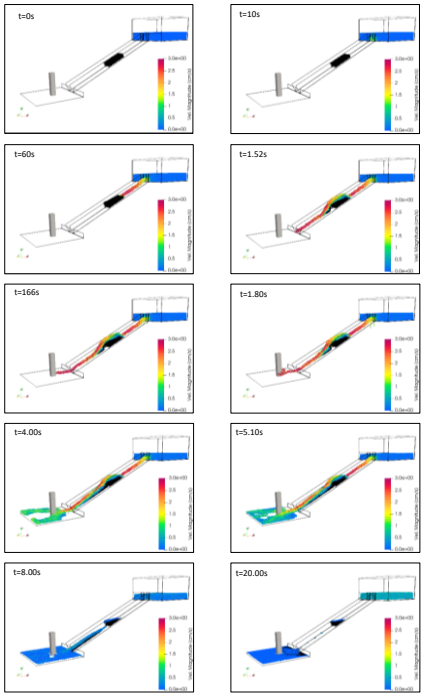

Fig. 9 - Velocity field of the simulation in different flow instants for Case 1B

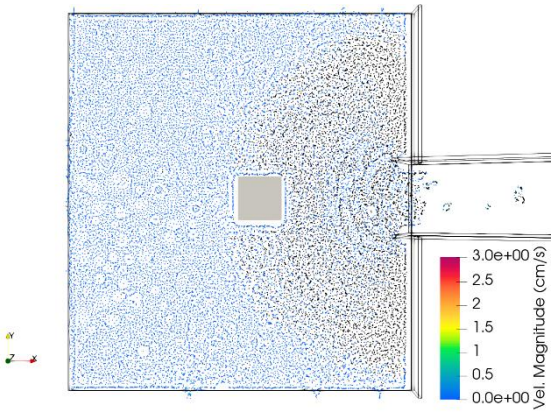

Fig. 10 - Simulation result of the debris deposition at t=20.00 s for Case 1B

3.2 Comparison Case 1A and 1B

This section is comparing the simulation data from the DualSPHysics model for both additional Case 1A and 1B.

The comparison parameters can be seen in Table 4. Total elements for Case 1A and 1B are the same, which is 500,899 elements is because no geometry has changed and only the operational of the gate is different. For case 1A, the water gate will be fully opened in 5 seconds and Case 1B will be half opened in 5 seconds. The simulation runtime for Case 1A was 1 hours 19 minutes and 33 seconds and 1 hours 25 minutes and 55 seconds for Case 1B. Both cases are simulated for 20 s. This shows that operational changes in the model do not make a significant difference on simulation run time.

Table 4 - Parameters for Case 1A and 1B

Case	Slope Angle (°)	Water level in water tank (m)	Water gate operation	Water gate open time (s)	Total elements	Simulation runtime (HH:MM:SS)	Time of simulation (s)
1A	25	0.2	Fully Open	5	500,899	1:19:33	20
1B	25	0.2	Half Open	5	500,899	1:25:55	20

Fig. 11 is showing the force from DualSPHysics for both cases. It can be seen on the Figure that debris hit the building block at 1.47 s for Case 1A and 0.19 s slower for Case 1B. The maximum force value recorded for Case 1A is 55.2 N at 1.96 s and mean is 5.45 N. The maximum force value recorded for Case 1B is 47.3 N at 1.67 s and mean is 3.24 N. The percentage difference of force mean value is 50.86 % difference.

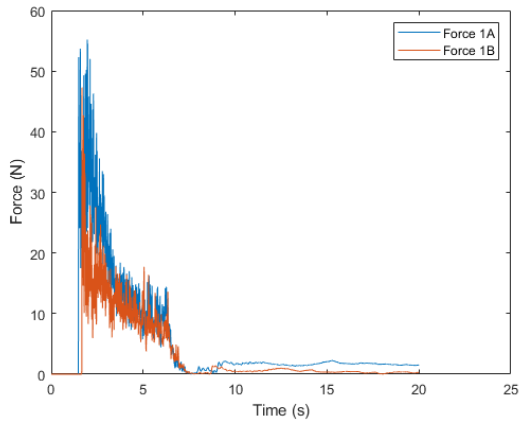

Fig. 11 - Plot of the force at building block for Case 1A and 1B in the DualSPHysics model

On the Fig. 12, the velocity magnitude from Dualspyhsic model for both cases can be seen. The velocity magnitude in the Case 1B model follows the values from the Case 1A very well. The velocity magnitude is very close, except for the large fluctuations at 5.57 until 6.40 s of the simulation. From the Fig. 12 it can be seen that the debris reached at 1.46 s for Case 1A and 1.69 s for Case 1B, the maximum velocity recorded for Case 1A is 3.44 cm/s at 3.46 s and 3.33 cm/s for Case 1B. The mean velocity is 0.41 cm/s for Case 1A and 0.10 cm/s higher than Case 1B. The percentage difference of velocity magnitude mean value is 27.78 % difference.

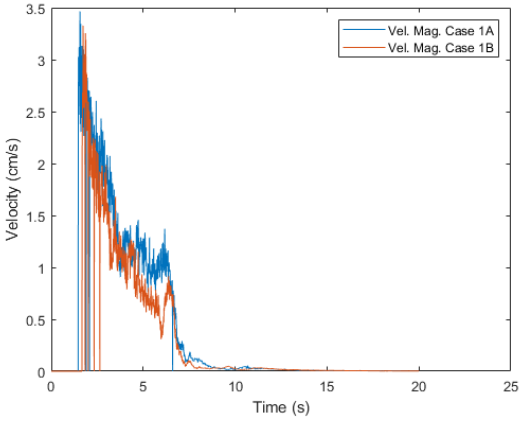

Fig. 12 - Plot of the velocity magnitude for Case 1A and 1B in the DualSPHysics model

From velocity magnitude graph, both cases go through the same three major stages as mentioned earlier; the acceleration stage after the mixture passes from the flume and reaches the monitoring point, the deceleration stage due to the viscosity of the mixture, and the propagation stage with a steady velocity. This shows that the volume of the fluid plays a role in the velocity fluctuations.

Furthermore, the graphs have the same tendency of the force, force mean value is reduced by more than half after the water gate is half opened. This is one more corroboration that the volume of the fluid plays a very important role in contributing to the changes of the velocity and force. The results comparison is made for both cases and can be seen in Table 5.

Table 5 - Results comparison for additional cases

Case	Force			Vel. Magnitude		
	Max. (N)	Mean (N)	Mean percentage difference (%)	Max. (cm/s)	Mean (cm/s)	Mean percentage difference (%)
1A	55.2	5.45	50.86	3.44	0.41	27.78
1B	47.3	3.24		3.33	0.31	

The Table 5 presents a comparison of force and velocity magnitudes between two cases, 1A and 1B. Case 1A exhibits a higher maximum force of 55.2 N and a mean force of 5.45 N. In contrast, Case 1B has a lower maximum force of 47.3 N and a mean force of 3.24 N. This indicates that Case 1A experiences greater forces overall. In terms of velocity magnitude, Case 1A also has higher values, with a maximum velocity of 3.44 cm/s and a mean of 0.41 cm/s. Meanwhile, Case 1B shows slightly lower velocity values, with a maximum of 3.33 cm/s and a mean of 0.31 cm/s. Overall, Case 1A consistently demonstrates greater force and velocity values compared to Case 1B.

In actual situation, the maximum impact force (5520 N) can be 100 times greater compared to model values (55.2 N). Imagine that during the event, structures at the deposition area were impacted by an impact force that was 100 times greater.

Experimental studies have quantified the impact forces, with Cui (2015) [46] reporting dynamic pressures ranging from 10–50 kPa and peak impact loads exceeding 2600 kPa in some cases. Such extreme forces can cause severe damage to structures if not adequately addressed in design. This highlights the need for structural designs that account for both the initial and sustained forces exerted by debris flows, ensuring that structures can withstand prolonged exposure to these dynamic forces.

4. CONCLUSSION

This study underscores the critical importance of quantitatively assessing debris flow impact forces to reduce risks to human life and property in susceptible areas. While the research primarily focused on simulating debris flow runout without directly modeling impact forces, the contrast between model values and actual forces—up to 100 times greater in real-world scenarios—highlights the significant potential for damage. Structures located in debris flow

deposition zones are particularly vulnerable, and the failure to accurately account for these forces could result in catastrophic consequences, including structural failure, significant financial losses, and loss of life.

The study's findings can play a pivotal role in guiding field interventions and informing disaster risk management strategies. Understanding the dynamics of debris flow forces, particularly the influence of factors like flow velocity, material composition, and slope, enables engineers to develop more robust structural designs. The integration of advanced modeling techniques, such as Smoothed Particle Hydrodynamics (SPH), provides deeper insights into debris flow behavior, helping to refine the design of protective barriers and other mitigation infrastructure. By applying these insights, engineers can optimize the placement and design of structures such as check dams, flexible barriers, and diversion channels to effectively absorb or redirect debris flow forces.

In terms of disaster risk management, the findings emphasize the need for a holistic approach that includes continuous monitoring, early warning systems, and community engagement. Early detection and real-time monitoring of debris flow events, using technologies such as remote sensing and sensor networks, are vital for activating timely response measures. This can significantly reduce the impact of debris flows by allowing for preemptive evacuations and protective actions. Additionally, implementing erosion control measures in upstream areas and managing sediment accumulation through regular maintenance of channels and reservoirs further reduces the likelihood of debris flow hazards.

The research also highlights the importance of educating and involving local communities in risk management efforts. Awareness programs can help residents understand the risks posed by debris flows and encourage proactive participation in disaster preparedness plans. Such community engagement, combined with the development of robust structural designs and early warning systems, will contribute to a comprehensive strategy for mitigating the impact of debris flows.

By integrating these findings into disaster risk management and field interventions, engineers, planners, and authorities can better protect infrastructure, reduce vulnerabilities, and enhance the resilience of communities located in debris flow-prone regions.

ACKNOWLEDGEMENT

Acknowledgement to "Ministry of Higher Education Malaysia under the Highest Institution Center of Excellence (HICOE) research grant (311.PREDAC.4403901) and Ministry of Higher Education Malaysia for Fundamental Research Grant Scheme with Project Code: FRGS/1/2016/TK01/USM/02/4."

References

[1] T. Takahashi, "A Review of Japanese Debris Flow Research," *Int. J. Eros. Control Eng.*, vol. 2, no. 1, pp. 1–14, 2009, doi: 10.13101/ijece.2.1.

[2] G. D. Zhou, R. P. H. Law, and C. W. W. Ng, "The mechanisms of debris flow: A preliminary study," *Proc. 17th Int. Conf. Soil Mech. Geotech. Eng. Acad. Pract. Geotech. Eng.*, vol. 2, pp. 1570–1573, 2009, doi: 10.3233/978-1-60750-031-5-1570.

[3] M. R. R. Mohd Arif Zainol and M. K. Awahab, "Hydraulic Physical Model of Debris Flow for Malaysia Case Study," in *IOP Conference Series: Materials Science and Engineering*, 2018, vol. 374, no. 1, doi: 10.1088/1757-899X/374/1/012067.

[4] D. Tiranti, S. Crema, M. Cavalli, and C. Deangeli, "An Integrated Study to Evaluate Debris Flow Hazard in Alpine Environment," *Front. Earth Sci.*, vol. 6, no. May, pp. 1–14, 2018, doi: 10.3389/feart.2018.00060.

[5] N. S. Muhammad, P. Y. Julien, and J. D. Salas, "Probability Structure and Return Period of Multiday Monsoon Rainfall," *J. Hydrol. Eng.*, vol. 21, no. 1, Jan. 2016, doi: 10.1061/(ASCE)HE.1943-5584.0001253.

[6] H. A. Rahman and J. Mapjabil, "Landslides Disaster in Malaysia: an Overview," *Heal. Environ. J.*, vol. 8, no. 1, pp. 58–71, 2017.

[7] E. Jr. Joe, F. Tongkul, and R. Roslee, "Engineering Properties of Debris Flow Material At Bundu Tuhan, Ranau, Sabah, Malaysia," *Pakistan J. Geol.*, vol. 2, no. 2, pp. 22–26, 2018, doi: 10.26480/pjg.02.2018.22.26.

[8] N. Kasim, K. A. Taib, M. Mukhlisin, and A. Kasa, "Triggering Mechanism and Characteristic of Debris Flow in Peninsular Malaysia," *Am. J. Enginering Res.*, vol. 5, no. 4, pp. 112–119, 2016.

[9] K. F. Liu and M. C. Huang, "Numerical simulation of debris flows," *Proc. Int. Conf. Offshore Mech. Arct. Eng. - OMAE*, vol. 6, pp. 375–382, 2009, doi: 10.1115/OMAE2009-79197.

[10] T. C. Chang, Z. Y. Wang, and Y. H. Chien, "Hazard assessment model for debris flow prediction," *Environ. Earth Sci.*, vol. 60, no. 8, pp. 1619–1630, 2010, doi: 10.1007/s12665-009-0296-x.

[11] M. li Li, Y. jun Jiang, T. Yang, Q. bing Huang, J. ping Qiao, and Z. ji Yang, "Early warning model for slope debris flow initiation," *J. Mt. Sci.*, vol. 15, no. 6, pp. 1342–1353, 2018, doi: 10.1007/s11629-017-4779-z.

[12] G. Vargas-Cuervo, E. Rotigliano, and C. Conoscenti, "Prediction of debris-avalanches and -flows triggered by a tropical storm by using a stochastic approach: An application to the events occurred in Mocoa (Colombia) on 1 April 2017," *Geomorphology*, vol. 339, no. December 1999, pp. 31–43, 2019, doi: 10.1016/j.geomorph.2019.04.023.

[13] J. W. Zhou, P. Cui, X. G. Yang, Z. M. Su, and X. J. Guo, "Debris flows introduced in landslide deposits under rainfall conditions: The case of Wenjiagou gully," *J. Mt. Sci.*, vol. 10, no. 2, pp. 249–260, 2013, doi: 10.1007/s11629-013-2492-0.

[14] S. C. Chen and C. Y. Wu, "Debris flow disaster prevention and mitigation of non-structural strategies in Taiwan," *J. Mt. Sci.*, vol. 11, no. 2, pp. 308–322, 2014, doi: 10.1007/s11629-014-2987-3.

[15] U. S. Lay and B. Pradhan, "Identification of debris flow initiation zones using topographic model and airborne laser scanning data," *Lect. Notes Civ. Eng.*, vol. 9, pp. 915–940, 2019, doi: 10.1007/978-981-10-8016-6_65.

[16] B. Pradhan and S. B. A. Bakar, "Debris Flow Source Identification in Tropical Dense Forest Using Airborne Laser Scanning Data and Flow-R Model BT - Laser Scanning Applications in Landslide Assessment," B. Pradhan, Ed. Cham: Springer International Publishing, 2017, pp. 85–112.

[17] M. Borga, M. Stoffel, L. Marchi, F. Marra, and M. Jakob, "Hydrogeomorphic response to extreme

rainfall in headwater systems: Flash floods and debris flows," *J. Hydrol.*, vol. 518, no. PB, pp. 194–205, 2014, doi: 10.1016/j.jhydrol.2014.05.022.

[18] C. Liu, X. Tang, H. Wei, P. Wang, and H. Zhao, "Model Tests of Jacked-Pile Penetration into Sand Using Transparent Soil and Incremental Particle Image Velocimetry," *KSCE J. Civ. Eng.*, vol. 24, no. 4, pp. 1128–1145, 2020, doi: 10.1007/s12205-020-1643-4.

[19] J. qi Zhuang, P. Cui, J. bing Peng, K. heng Hu, and J. Iqbal, "Initiation process of debris flows on different slopes due to surface flow and trigger-specific strategies for mitigating post-earthquake in old Beichuan County, China," *Environ. Earth Sci.*, vol. 68, no. 5, pp. 1391–1403, 2013, doi: 10.1007/s12665-012-1837-2.

[20] M. Boreggio, M. Bernard, and C. Gregoretti, "Evaluating the differences of gridding techniques for Digital Elevation Models generation and their influence on the modeling of stony debris flows routing: A case study from Rovina di Cancia basin (North-eastern Italian Alps)," *Front. Earth Sci.*, vol. 6, p. 89, 2018.

[21] Z. F. Wang, X. S. Zhang, X. Z. Zhang, M. T. Wu, and B. Wu, "Hazard assessment of potential debris flow: A case study of Shaling Gully, Lingshou County, Hebei Province, China," *Front. Earth Sci.*, vol. 11, p. 1089510, 2023.

[22] S. M. Hsu, L. B. Chiou, G. F. Lin, C. H. Chao, H. Y. Wen, and C. Y. Ku, "Applications of simulation technique on debris-flow hazard zone delineation: a case study in Hualien County, Taiwan," *Nat. Hazards Earth Syst. Sci.*, vol. 10, no. 3, pp. 535–545, Mar. 2010, doi: 10.5194/nhess-10-535-2010.

[23] S. Bosa, M. Petti, S. Pascolo, and C. Reolon, "A New Approach to Debris Flow Study," *IOP Conf. Ser. Mater. Sci. Eng.*, vol. 603, no. 3, p. 32068, 2019, doi: 10.1088/1757-899X/603/3/032068.

[24] S. Piche, I. Nistor, and T. Murty, "Numerical modeling of debris impacts using the SPH method," *Coast. Eng. Proc*, vol. 1, no. 34, p. 19, 2014.

[25] H. Park, M.-J. Koh, D. T. Cox, M. S. Alam, and S. Shin, "Experimental study of debris transport driven by a tsunami-like wave: Application for non-uniform density groups and obstacles," *Coast. Eng.*, vol. 166, p. 103867, 2021, doi: https://doi.org/10.1016/j.coastaleng.2021.103867.

[26] Z. Han *et al.*, "Numerical simulation of debris-flow behavior based on the SPH method incorporating the Herschel-Bulkley-Papanastasiou rheology model," *Eng. Geol.*, vol. 255, pp. 26–36, 2019, doi: https://doi.org/10.1016/j.enggeo.2019.04.013.

[27] M. A. W. Khairi, M. R. Rozainy, and J. Ikhsan, "Smoothed particle hydrodynamics simulation for debris flow: a review," in *AIP Conference Proceedings*, 2020, vol. 2291, no. 1.

[28] S. M. Tayyebi *et al.*, "Two-phase SPH modelling of a real debris avalanche and analysis of its impact on bottom drainage screens," *Landslides*, vol. 19, no. 2, pp. 421–435, 2022, doi: 10.1007/s10346-021-01772-9.

[29] Z. Dai, F. Wang, Y. Huang, K. Song, and A. Iio, "SPH-based numerical modeling for the post-failure behavior of the landslides triggered by the 2016 Kumamoto earthquake," *Geoenvironmental Disasters*, vol. 3, no. 1, 2016, doi: 10.1186/s40677-016-0058-5.

[30] G.-R. Liu and M. B. Liu, *Smoothed particle hydrodynamics: a meshfree particle method*. World scientific, 2003.

[31] M. B. Liu and G. Liu, "Smoothed particle hydrodynamics (SPH): an overview and recent developments," *Arch. Comput. methods Eng.*, vol. 17, pp. 25–76, 2010.

[32] M. Gomez-Gesteira, B. D. Rogers, A. J. C. Crespo, R. A. Dalrymple, M. Narayanaswamy, and J. M. Dominguez, "SPHysics - development of a free-surface fluid solver - Part 1: Theory and formulations," *Comput. Geosci.*, vol. 48, pp. 289–299, 2012, doi: 10.1016/j.cageo.2012.02.029.

[33] X. F. Yang, S. L. Peng, and M. B. Liu, "A new kernel function for SPH with applications to free surface flows," *Appl. Math. Model.*, vol. 38, no. 15–16, pp. 3822–3833, 2014, doi: 10.1016/j.apm.2013.12.001.

[34] C. Johnson, B. P. Kokelaar, R. M. Iverson, M. Logan, R. G. LaHusen, and J. O. Gray, "Grain-size Segregation and Levee Formation in Geophysical Mass Flows," *J. Geophys. Res. Atmos.*, vol. 117, no. F1, 2012, doi: 10.1029/2011jf002185.

[35] H. X. Chen, J. Li, S. J. Feng, H. Y. Gao, and D. M. Zhang, "Simulation of interactions between debris flow and check dams on three-dimensional terrain," *Eng. Geol.*, vol. 251, no. August 2018, pp. 48–62, 2019, doi: 10.1016/j.enggeo.2019.02.001.

[36] Z. Dai, Y. Huang, H. Cheng, and Q. Xu, "SPH model for fluid–structure interaction and its application to debris flow impact estimation," *Landslides*, vol. 14, no. 3, pp. 917–928, 2017, doi: 10.1007/s10346-016-0777-4.

[37] S. J. Feng, H. Y. Gao, L. Gao, L. M. Zhang, and H. X. Chen, "Numerical modeling of interactions between a flow slide and buildings considering the destruction process," *Landslides*, vol. 16, no. 10, pp. 1903–1919, 2019, doi: 10.1007/s10346-019-01220-9.

[38] C. Liu, Z. Yu, and S. Zhao, "A coupled SPH-DEM-FEM model for fluid-particle-structure interaction and a case study of Wenjia gully debris flow impact estimation," *Landslides*, vol. 18, no. 7, pp. 2403–2425, 2021, doi: 10.1007/s10346-021-01640-6.

[39] C. Liu, Z. Yu, and S. Zhao, "Consideration of maximum impact force design for a rock shed against dry granular flow," *Eur. J. Environ. Civ. Eng.*, vol. 26, no. 7, pp. 2963–2984, 2022, doi: 10.1080/19648189.2020.1779135.

[40] K. Wu, D. Yang, N. Wright, and A. Khan, "An integrated particle model for fluid–particle–structure interaction problems with free-surface flow and structural failure," *J. Fluids Struct.*, vol. 76, pp. 166–184, 2018, doi: 10.1016/j.jfluidstructs.2017.09.011.

[41] H. Xiang and B. Chen, "A Moving Particle Semi-implicit Method for Free Surface Flow: Improvement in Inter-particle Force Stabilization and Consistency Restoring," *Int. J. Numer. Methods Fluids*, vol. 84, no. 7, pp. 409–442, 2016, doi: 10.1002/fld.4354.

[42] C. A. D. F. Filho, D. F. Pezzin, and J. T. A. Chacaltana, "A Numerical Study of Heat Diffusion Using the Lagrangian Particle SPH Method and the Eulerian Finite-Volume Method: Analysis of Convergence, Consistency and Computational Cost," 2014, doi: 10.2495/ht140021.

[43] Z. Zhang, W. Zhang, Z. J. Zhai, Q. Y. Chen, Z. J. Zhai, and Q. Y. Chen, "Evaluation of Various Turbulence Models in Predicting Airflow and Turbulence in Enclosed Environments by CFD : Part 2 — Comparison with Experimental Data from Literature Evaluation of Various Turbulence Models in Predicting Airflow and Turbulence in Enclo," *HVAC&R Res.*, vol. 9669, no. February 2016, pp. 37–41, 2011.

[44] T. C. Chang and Y. H. Chien, "The application of genetic algorithm in debris flows prediction," *Environ. Geol.*, vol. 53, no. 2, pp. 339–347, 2007, doi: 10.1007/s00254-007-0649-2.

[45] D. G. Lin, S. Y. Hsu, and K. T. Chang, "Numerical simulations of flow motion and deposition characteristics of granular debris flows," *Nat. Hazards*, vol. 50, no. 3, pp. 623–650, 2009, doi: 10.1007/s11069-009-9371-6.

[46] P. Cui, C. Zeng, and Y. Lei, "Experimental Analysis on the Impact Force of Viscous Debris Flow," *Earth Surf. Process. Landforms*, vol. 40, no. 12, pp. 1644–1655, 2015, doi: 10.1002/esp.3744.